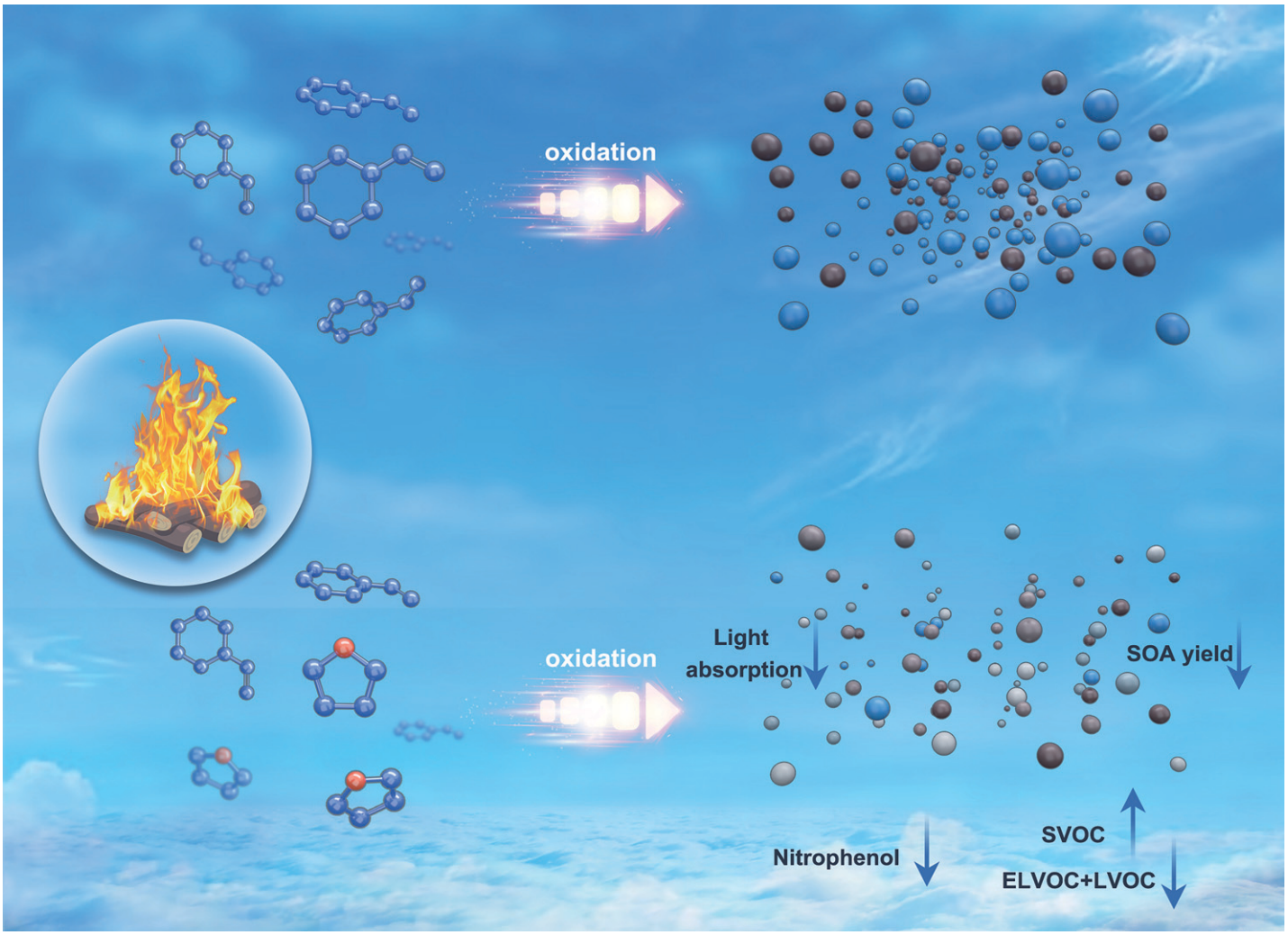

Showcasing research from Professor Kun Li's laboratory, Environment Research Institute, Shandong University, Qingdao, China.

Chemical interactions within biomass-burning emissions significantly influence the composition and optical properties of nanoscale secondary organic aerosols

This study shows how chemical interactions between furan and styrene (two typical biomass-burning VOCs) influence the formation and light-absorbing properties of nanoscale secondary organic aerosol (SOA). The co-oxidation of styrene and furan yields lower SOA mass and reduced light absorption, attributed to inhibited formation of nitrophenolic chromophores and low-volatility dimers. These findings underscore the need to incorporate VOC interaction effects into atmospheric models for a more accurate assessment of aerosol impacts on climate and air quality.

Image reproduced by permission of Kun Li from *Environ. Sci.: Nano*, 2026, **13**, 257.

As featured in:

See Kun Li *et al.*, *Environ. Sci.: Nano*, 2026, **13**, 257.

ROYAL SOCIETY OF CHEMISTRY

rsc.li/es-nano

Registered charity number: 207890

Environmental Science Nano

ROYAL SOCIETY OF CHEMISTRY

PAPER

View Article Online
View Journal | View Issue

Cite this: *Environ. Sci.: Nano*, 2026, **13**, 257

Chemical interactions within biomass-burning emissions significantly influence the composition and optical properties of nanoscale secondary organic aerosols

Shan Zhang,[ab] Kun Li, *[a] Li Xu[a] and Lin Du [a]

Received 18th August 2025,
Accepted 7th November 2025

DOI: 10.1039/d5en00770d

rsc.li/es-nano

Biomass burning (BB) emits a substantial amount of trace gases, and their atmospheric oxidation makes a large contribution to secondary organic aerosol (SOA) formation. However, the potential interactive effect of mixed volatile organic compounds (VOCs) from BB on SOA formation remains largely unknown. Here, we studied the molecular composition and optical properties of nanoscale SOA formed from the mixture of two typical VOCs in BB emissions (styrene and furan) with distinct chemical characteristics. The ratio of furan to styrene was controlled within a range of 0.5–10, based on actual emission ratios. By investigating SOA variations at the molecular level, we found that the SOA yield and light absorption in the furan–styrene mixture system were significantly lower than those in the styrene system. The decrease in SOA yield in the mixture experiments might be explained by changes in the distribution of organic aerosol components. Specifically, the addition of furan reduced the proportion of low-volatility organic compounds and increased the proportion of semi-volatile organic compounds. Tandem mass spectrometry (MS/MS) analysis indicated that the reduction in light absorption after furan addition could be attributed to the suppressed formation of nitrophenolic compounds, since typical chromophores such as $C_6H_5NO_3$ and $C_6H_5NO_4$ were only identified in styrene SOA. These findings highlight the complex interactions between organic gases in BB emissions and their significant impact on SOA formation and optical properties.

Environmental significance

Chemical interactions among biomass-burning volatile organic compounds (VOCs) play a critical role in shaping the composition and optical properties of nanoscale secondary organic aerosols (SOA). Our results demonstrate that furan–styrene interactions significantly suppress SOA yield by reducing the formation of low-volatility compounds, while simultaneously suppressing light absorption through the inhibition of nitrophenolic chromophores. These nanoscale molecular processes reveal that SOA derived from complex mixtures cannot be simply predicted from single-precursor behavior. By explicitly identifying the nanoscale pathways responsible for altered SOA composition and light absorption, this study emphasizes the necessity of incorporating chemical interaction effects into air quality and climate predictions, providing a more accurate assessment of biomass-burning impacts on the environment.

1. Introduction

Biomass burning (BB), including wildfires, agricultural residue combustion, and domestic heating, is a significant source of various volatile organic compounds (VOCs) and aerosols in the atmosphere.[1] BB emissions are estimated to account for approximately 90% of the global primary organic carbon emissions from all combustion sources.[2] The VOCs released from BB undergo complex chemical reactions in the atmosphere, leading to the formation of secondary organic aerosols (SOA),[3,4] which in turn influence the optical properties of aerosols and contribute to climate change.[5,6]

The concentrations of SOA in BB regions were underestimated by early regional air quality models.[7–9] SOA formation in these regions is highly complex, as the VOC emissions of BB consist of a diverse mixture of compounds that can vary significantly depending on the type of fuel and the fire characteristics.[10] Previous studies have predominantly focused on the molecular composition or optical properties of SOA derived from single precursor compounds such as furan, phenol, aromatic hydrocarbons,

[a] *Qingdao Key Laboratory for Prevention and Control of Atmospheric Pollution in Coastal Cities, Environment Research Institute, Shandong University, Qingdao, 266237, China. E-mail: kun.li@sdu.edu.cn*
[b] *Junji College, Henan Medical University, Xinxiang, 453003, China*

etc.[11–13] These studies provide a foundational understanding of individual precursor behavior in SOA formation. However, recent studies have indicated that the mass and yield of SOA formed from individual precursors may be influenced by the presence of other VOCs.[14–17] VOC mixtures from BB may interact in complex ways,[18,19] making the process far more intricate than single precursors. Correspondingly, the physical and chemical properties of SOA would be quite different from that formed from a single precursor.

Furan and styrene are two predominant compounds in BB emissions with distinct chemical characteristics.[20–22] The oxidation of styrene or furan has been widely investigated in previous studies,[23–26] and SOA formed from the oxidation of styrene or furan both exhibit significant light-absorbing capacity. In contrast, little is known about the formation and optical properties of SOA generated from the oxidation of furan–styrene mixtures. This limits a more nuanced understanding of the interactions among multiple VOCs in biomass-burning emissions.

Smog chambers and oxidation flow reactors (OFRs) are key laboratory tools for simulating atmospheric oxidation of VOCs and SOA formation.[27,28] Smog chambers typically maintain near-ambient OH levels suitable for simulating low-to-moderate degrees of oxidation. Some urban environments exhibit substantially elevated OH concentrations capable of driving high degrees of oxidation equivalent to >1 week of photochemical aging.[29,30] For this condition, OFRs are more suitable because they could provide high-degree-of-oxidation simulations by producing high concentrations of oxidants. In other words, OFRs are capable of simulating long photochemical ages, whereas smog chambers represent short photochemical ages. Therefore, integrating smog chambers with OFRs becomes essential to provide oxidation conditions covering low to high OH environments comprehensively.

Therefore, this study combines a smog chamber and an OFR to analyze the molecular composition and optical properties of SOA from furan–styrene mixtures under low and high degrees of oxidation (over tens of hours and over a hundred hours, respectively). The concentration ratio of furan to styrene ([furan]/[styrene]) was controlled in a wide range (0.5–10), reflecting the various emission ratios from different fuel combustion.[19,21,22,31] By investigating the oxidation pathways, products, and optical properties of SOA from furan–styrene mixtures, this study deepens our understanding of SOA formation and impacts from BB.

2. Methods

The oxidation experiments were conducted in two different laboratory settings (smog chamber and OFR), which provide a comparison between low and high degrees of oxidation for the furan–styrene mixed system (Fig. S2). The two facilities and the experiments conducted are described below.

2.1. Smog chamber experiments

A 1.5 m^3 chamber made of Teflon was used in this study. Before each experiment run, particles in the smog chamber were cleaned to be less than 1 μg m^{-3} by zero air from a zero-air generator (XHZ2000B, Xianhe).[27,32] Next, styrene (99.5%, Alfa Aesar) and furan (99%+, Adamas-beta) were added into the chamber carried by zero air, followed by the injection of H_2O_2 to generate sufficient hydroxyl radicals in photochemical reactions. Subsequently, wet zero air was introduced into the chamber to adjust relative humidity (RH) in the chamber to 50 ± 3%, and NO (500 ppm, DeYi) was added into the chamber to create a high NO_x condition. After all the gases were introduced, the chamber was irradiated by UV lamps (F40BLB, General Electric Company) with a central wavelength of 340 nm. The reaction time was 110 min for the separate and mixed experiments of styrene and furan. The average OH concentration was calculated by the decay of precursors, as described in section S2. The equivalent photochemical ages were from 4 h to 20 h. Ammonium sulfate particles were used to characterize particle wall losses (section S1).

For the online analysis, the NO_x concentration, RH, temperature (T), and the light absorption and scattering of aerosol particles were analyzed by NO_x analyzer (Model 42i, Thermo Fisher), RH/T sensor (HM40, Vaisala, Finland), and photoacoustic extinctiometer (PAX), respectively. The size distribution of aerosol was measured with a scanning mobility particle sizer (SMPS), which consists of a differential mobility analyzer (DMA) (55-L, Grimm, Germany) and a condensation particle counter (CPC) (5416, Grimm, Germany). The concentration of styrene and furan were analyzed by a gas chromatograph (GC, 7890B, Agilent Technologies, USA) equipped with a DB624 column (30 m × 0.32 mm, 1.8 μm film thickness, Agilent Technologies, USA), and the GC temperature program was ramped from 80 to 200 °C at a rate of 20 °C min^{-1}. For the offline analysis, the SOA particles were collected using Teflon filters. The filters were cut into half, one half was used for light absorption analysis by ultraviolet-visible spectroscopy (UV-vis) (P9, Shanghai Mapada, China), while the other half was used for chemical composition and light absorption analysis by Ultra-Performance Liquid Chromatography coupled with a DAD detector and a Quadrupole Time-of-Flight Mass spectrometer (UPLC-DAD-Q-TOF-MS) (Bruker Impact HD, Germany). More details about chemical characterization and data analysis can be seen in SI.

2.2. OFR experiments

The high-degree-of-oxidation experiments were carried out in an OFR described previously.[33,34] The inner wall surface of the reactor was coated with Teflon FEP film (0.5 mm thickness). This Teflon coating has excellent chemical stability and anti-aging properties and is often used as an anti-stick coating to reduce wall reactivity.[35] The ratio of wet zero air and dry zero air was adjusted to maintain a stable

RH (~50%). The O_3 in the reactor (5 ppm) was produced by an O_3 generator (UV-M2, Beijing Tonglin). Styrene and furan were introduced into the reactor by flowing zero air through a vial filled with saturated vapor. At last, the OH radicals were produced by ozone photolysis in the presence of water vapor (*i.e.*, $O_3 + h\nu$ (254 nm) → $O(^1D) + O_2$, $O(^1D) + H_2O \rightarrow 2OH$). The UV lamp (Analytikjena, 90-0004-01, λ_{max} = 254 nm) was located inside a quartz tube in the OFR, and a flow of 10 L min^{-1} zero air was used to sweep away the heat. To evaluate the contribution of direct photolysis to SOA formation from styrene or furan under 254 nm irradiation, we performed control experiments in which the precursor was continuously irradiated in the absence of an oxidant. As shown in Fig. S3, these experiments revealed only minimal particle production from photolysis alone. In contrast, the introduction of O_3 (as a source of OH radicals) resulted in substantial SOA yields. To create a high NO_x condition, pure N_2O at a volumetric flow ratio of 0.2–0.3% was introduced into the flow reactor (*i.e.*, $N_2O + O(^1D) \rightarrow NO$), making 90% of RO_2 react with NO. OH concentration was adjusted by tuning the input voltage of the UV lamp. The OH exposure was calculated according to CO decay measured by a CO analyzer (Model 48i, Thermo Fisher) (section S2).

Experimental overviews, including VOC and NO_x concentrations, particle mass concentrations, SOA yields, temperature, relative humidity, equivalent photochemical ages, and the real part and the imaginary part of complex refractive index (measured and predicted value), are presented in Table S1.

3. Results and discussion

3.1. SOA formation

The variations in mass concentration and SOA yield with increasing [furan]/[styrene] ratios are shown in Fig. 1 and Table S1. The mass concentration increased with [furan]/[styrene] ratios in both the smog chamber and OFR (Fig. 1a). However, the yield of styrene–furan SOA decreased as the furan concentration increased (Fig. 1b). It is important to recognize that the mass concentration will naturally rise when an additional VOC precursor is introduced into the system. Since the SOA yield of furan was lower than that of styrene, the mixed SOA yield was decreased due to the dilutive effect. To clarify whether the reduction in mixed SOA yields is solely attributed to the dilution effect of lower-yield furan, the predicted SOA yield values were calculated under the assumption of no chemical effects (calculation method in section S3) and compared with the measured SOA yield values. It should be noted that the prediction of SOA yield must be conducted within similar equivalent photochemical age ranges for each reaction system. Therefore, the equivalent photochemical age in the smog chamber was controlled at approximately 10 hours, while in the OFR, it was controlled at around 200 hours. It shows that the measured SOA yields in both the smog chamber and the OFR were slightly lower than the predicted values (Fig. 1b and Table S1). This suggests that the reduction in SOA yields in the mixed system is related to the interaction between furan and styrene. Additionally, the number concentration of styrene–furan SOA decreased compared to the styrene-only system both in the smog chamber and OFR (see Fig. S4 and S5). This result suggests that the addition of furan may have suppressed the formation of certain low-volatility compounds, leading to a decrease in the number concentration. The relevant mechanisms will be further discussed in the following sections.

3.2. Molecular composition and volatility changes induced by styrene–furan interactions

To explore the reason for the decreased SOA number concentration, yield, and light absorption with the addition of furan, we compared the SOA composition with and without furan. As shown in Fig. 2a, 944 compounds were detected in styrene SOA, while 437 compounds were found in styrene–furan SOA. In addition to 139 overlapping compounds, there are 805 unique compounds for styrene SOA and 298 unique compounds for styrene–furan SOA. Furthermore, we compared the distinction of these unique compounds. As we can see in Fig. 2b, the average O/C (0.99) of unique compounds in styrene–furan SOA is lower than that (1.18) in styrene SOA in the smog chamber. Correspondingly, we also compared the unique compounds in OFR experiments; it is interesting to note that the average

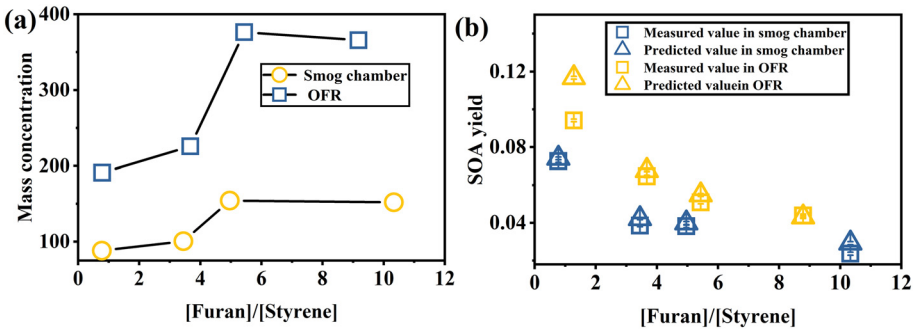

Fig. 1 The variation for mass concentration (a) and SOA yield (with error bar) (b) across different furan-to-styrene concentration ratios in both smog chamber and OFR experiments.

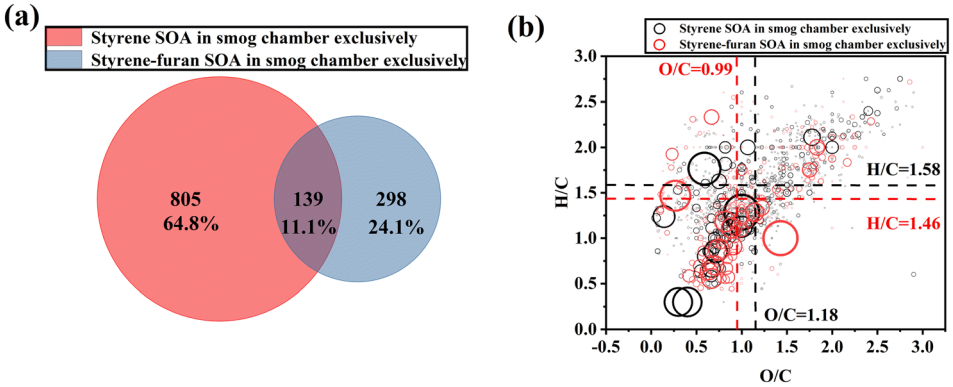

Fig. 2 (a) Venn diagram illustrating the overlap and unique compounds between styrene SOA and styrene–furan SOA in the smog chamber. (b) Van Krevelen diagram depicting the unique compounds formed during styrene and styrene–furan OH oxidation in the smog chamber. The size of the circles represents the relative intensity.

O/C (0.83) of unique compounds in styrene–furan SOA is likewise lower than that (0.91) in styrene SOA under higher degrees of oxidation (Fig. S6). The lower O/C in styrene–furan unique SOA indicates a decrease in oxidation state when adding furan to the reaction system.

Furthermore, we classified highly oxygenated molecules (HOMs) based on the criteria established in previous studies, defining HOMs as compounds with an O/C ratio greater than 0.6.[36] Using this classification, we calculated and visualized the relative intensity of HOMs in unique styrene SOA and styrene–furan SOA (Fig. 3a). The relative intensity of HOMs in unique styrene–furan SOA is lower than that in styrene SOA in the smog chamber experiments and approximately comparable in the OFR experiments. In addition, according to the saturation mass concentration (C_0) of pure compound, we have divided the SOA components into four groups: intermediate volatile organic compounds (IVOCs: $300 < C_0 < 3 \times 10^6$ μg m^{-3}), semi volatile organic compounds (SVOCs: $0.3 < C_0 < 300$ μg m^{-3}), low-volatile organic compounds (LVOCs: $3 \times 10^{-4} < C_0 < 0.3$ μg m^{-3}), and extremely low-volatile

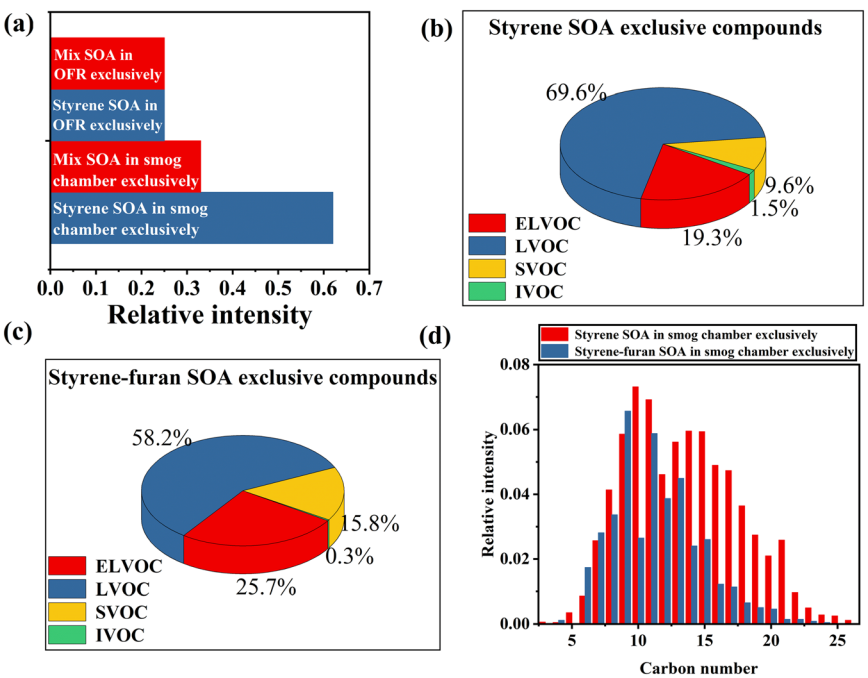

Fig. 3 Comparison of unique compounds in styrene OH oxidation and styrene–furan OH oxidation. (a) Relative intensity of highly oxygenated molecules (HOMs) (sum of observed intensity of all HOMs identified in the unique compound set for each system, normalized to the total observed intensity of all detected compounds in that sample). (b) Proportional distribution of intermediate volatile organic compounds (IVOCs), semi volatile organic compounds (SVOCs), low-volatile organic compounds (LVOCs), and extremely low-volatile organic compounds (ELVOCs) in SOA from styrene OH oxidation (unique compounds). (c) Proportional distribution of IVOCs, SVOCs, LVOCs, and ELVOCs in styrene–furan unique SOA. (d) Variation in the relative intensity of unique compounds with carbon number in styrene and styrene–furan OH radical oxidation systems.

organic compounds (ELVOCs: $C_0 < 3 \times 10^{-4}$ μg m^{-3}) (the detailed calculation method can be seen in section S6).[37] It can be found that the proportion of LVOC + ELVOC from unique styrene SOA to styrene–furan SOA decreased from 69.6% to 58.19%, and SVOC increased from 19.3% to 25.73% in the smog chamber (Fig. 3b and c). Similarly, the proportion of LVOC + ELVOC from unique styrene SOA to styrene–furan SOA decreased from 66.7% to 61.4%, and SVOC increased from 5.86% to 13.76% in the OFR (Fig. S7). From the carbon number distribution (Fig. 3d), we found that the C_9–C_{12} compounds dominate the unique styrene SOA and styrene–furan SOA, while the relative intensity of $>C_{12}$ compounds in styrene is higher than that in styrene–furan SOA. These results indicate that the addition of furan favors the formation of low-molecular-weight and more volatile products, leading to lower SOA yields.

To clarify the dominant LVOC + ELVOC compounds in styrene-unique SOA and the SVOC compounds in styrene–furan-unique SOA, we identified some major compounds. As shown in Table S2 (taking the smog chamber experiments as an example), representative LVOC and ELVOC compounds in the styrene-unique SOA predominantly fall within the C_9–C_{16} range, similar to the carbon number distribution presented in Fig. 3. It was observed that the LVOC compounds in the C_9–C_{12} range of unique styrene SOA are primarily nitro-substituted compounds, while the $>C_{12}$ compounds are mainly dimers resulting from styrene oxidation. We hypothesize that the addition of furan may inhibit the formation of nitrogenous compounds and low-volatility dimers of styrene, thereby reducing SOA formation. Regarding the higher light absorption observed during styrene OH oxidation, we proposed that nitrophenols in styrene SOA play a significant role in light absorption. It has been identified that $C_6H_5NO_3$, $C_6H_5NO_4$, and $C_6H_5NO_5$ were the primary BrC chromophores formed during styrene OH oxidation[23] (see it in Fig. S8). In addition, these compounds demonstrate the high light-absorbing properties in previous studies.[38–41] Furthermore, these compounds have been found to exhibit high light absorption in our previous work.[23] These three C_6 nitrophenols were detected uniquely in the styrene SOA in this study, but were absent in the styrene–furan SOA. This suggests that the presence of furan might inhibit their formation, likely through reactions between furan oxidation intermediates and styrene intermediates, thereby reducing the overall light absorption in the styrene–furan SOA. In contrast, the majority of SVOC and IVOC compounds in the

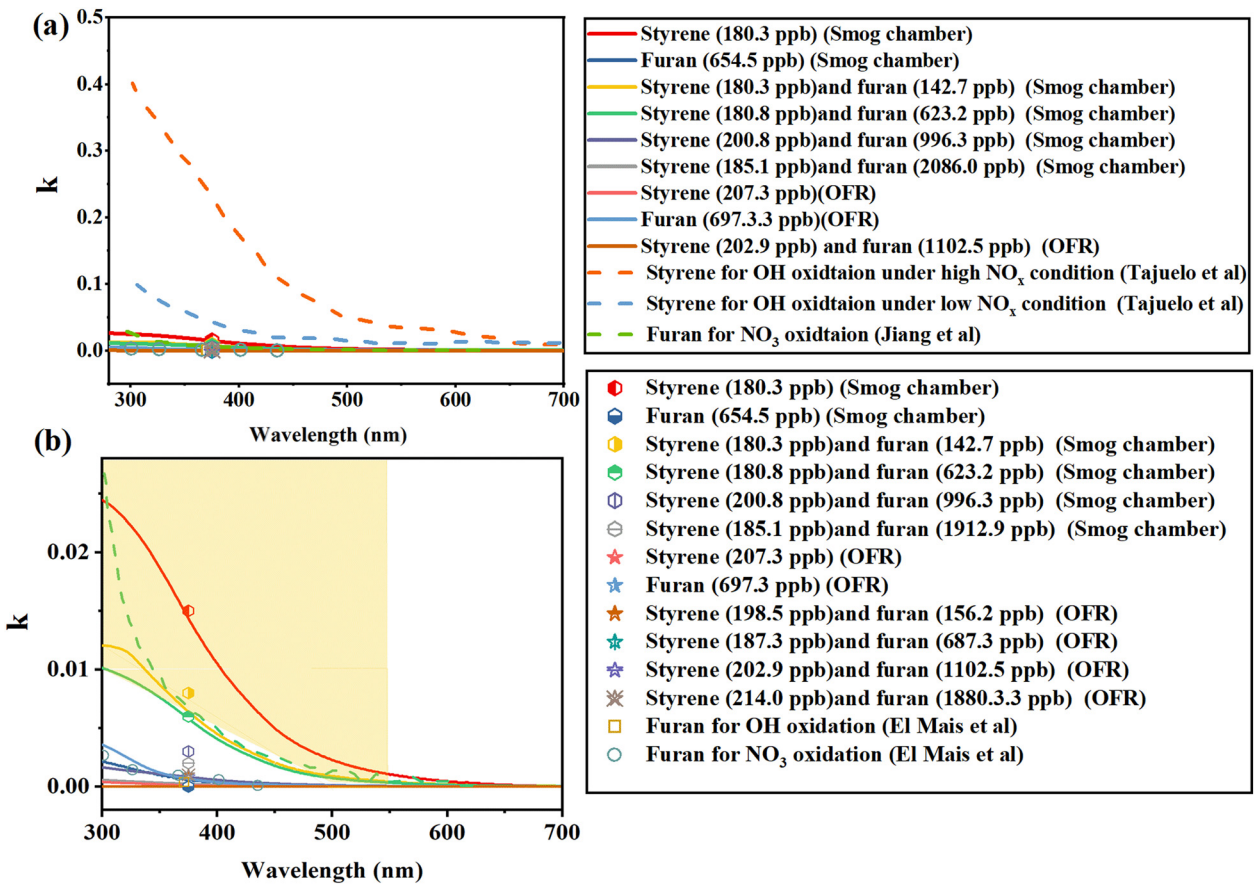

Fig. 4 Comparison of light-absorbing properties of SOA formed under varying furan-to-styrene concentration ratios in the smog chamber and OFR. (a) *k* values across the 300–700 nm measured by PAX and UV-vis techniques, compared with literature data for styrene/furan oxidation in previous studies.[24–26] (b) The zoomed-in view, where the brown-shaded region represents the typical range of BrC as reported previously[38] (zoomed-in view of the light absorption curves for regions with lower *k*-values was in Fig. S12).

styrene–furan-unique SOA are CHO species (Table S2), which are likely formed through reactions between furan intermediates or between furan and styrene intermediates.

3.3. Optical properties and their link to molecular composition

The chemical interactions and suppressed formation of nitrophenolic chromophores in the furan–styrene system (section 3.2) are manifested in the bulk optical properties of the SOA. We find that the mixed SOA exhibits significantly reduced light absorption compared to the prediction based on single-precursor behavior. As we can see in Fig. 4, the optical properties of styrene and styrene–furan SOA were measured using both online and offline technique. Online measurements *via* PAX allow for real-time tracking of changes in aerosol optical properties during oxidation, whereas offline measurements *via* UV-vis provide detailed data on light absorption across a wide range of wavelengths. In the online analysis (Fig. S9 and S10), the aerosol light absorption/scattering coefficient increased as the smog chamber reaction progressed. Additionally, the imaginary part of the complex refractive index (k) decreased with increasing furan–styrene ratio in the smog chamber (Fig. 4b), indicating that mixing with furan reduced the light absorption of SOA. The k values in the smog chamber were higher than those in the OFR as a whole. We attribute this behavior to a shift from functionalization to fragmentation with increasing oxidation degree, which reduces the light-absorbing capacity at higher levels of oxidation.[36,37] For offline analysis using UV-vis, the k value was derived from the MAC (refer to section S4). A comparison of the k values at 375 nm obtained *via* PAX and UV-vis spectroscopy (Fig. 4b) demonstrated strong consistency between the online and offline methods, confirming the reliability of the results. Additionally, the k value with increased furan addition in the smog chamber, as well as the k value observed in the OFR, both fell outside the BrC regions (brown areas in Fig. 4b). In addition, we compared the light absorption properties of styrene-derived SOA and furan-derived SOA reported in the previous studies.[24–26] For styrene SOA, the k-value in previous study[26] was higher than the k-value analyzed in this work, which may be due to the difference in oxidant types and experimental conditions.[23] As for furan, the k-value of furan OH oxidation in previous studies was relatively close to the results obtained in this study, both showing lower light absorption.[24,25] Overall, SOA generated from styrene exhibited higher light absorption than SOA generated from furan.

To investigate whether the decrease in the k value of the mixed products is solely attributable to the dilutive effect of furan or to chemical interactions, we calculated the predicted k values (section S4) without considering chemical interactions. As shown in Fig. S11, the measured k values, whether derived from online measurements (PAX) or offline analysis (UV-vis), were consistently lower than the predicted k value. This indicates that the reduction in the k value is not merely due to the addition of furan with lower light absorption but also involves interactions between oxidation products from styrene and furan, which are further explored at the molecular level in the following sections.

3.4. Possible mechanism leading to the composition difference

Taking this further, we propose possible structures based on their accurate m/z and fragmentation mass spectra, taking the compounds in the styrene-unique SOA as an example (Fig. 5). Among these compounds, the fragmentations of monomers $C_6H_5NO_3$, $C_6H_5NO_4$, $C_6H_5NO_5$, $C_9H_6O_5$, and $C_9H_6N_2O_7$ were similar (Fig. 5a–e). Taking $C_6H_5NO_3$ as an example, the fragmentation of the parent ion $C_6H_4NO_3^-$ (m/z 138.0197) led to the neutral loss of 30 Da (NO), forming a fragment ion ($C_6H_4O_2^-$) at m/z 108.0215 (Table S3a), consistent with the cleavage of a NO group previously reported for 4-nitrophenol.[42] Generally, compounds containing an NO_2 group tend to undergo neutral losses of NO (30 Da), NO_2 (46 Da), or HNO (31 Da) in negative-ion MS/MS spectra.[43,44] In this study, the neutral loss of NO was observed for parent ions $C_6H_4NO_3^-$, $C_9H_5N_2O_7^-$, $C_{12}H_6NO_4^-$, and $C_6H_4NO_4^-$ (Table S3), while the neutral loss of NO_2 was observed in $C_9H_5N_2O_7^-$, $C_{12}H_6NO_4^-$, and $C_6H_4NO_5^-$ (Table S3). Similarly, the neutral loss of HNO was identified for $C_6H_4NO_4^-$ and $C_6H_4NO_5^-$ (Table S3). Additionally, carboxylate anions $[M–H]^-$ typically undergo losses of CO_2 or H_2O,[43,45] as observed in $C_9H_5N_2O_7^-$ and $C_9H_5O_5^-$ (Table S3). Compounds with OH groups generally lose H_2O (18 Da).[46] Apart from the fragmentation of monomers, the number of fragment ions of dimers is generally limited, and determining the exact structure of dimers is more uncertain compared to monomers.[47] For example, the oligomer ion $C_{10}H_8NO_7^-$ (m/z 253.9057) underwent a cleavage of the ester bond, resulting in the monomeric fragments ($C_6H_4NO_4^-$) at m/z 154.0199, and then it loses a NO to form a peak ion ($C_6H_4NO_3^-$) at m/z 124.0399 (Table S3). This fragmentation pattern also happened in $C_{10}H_9N_2O_7^-$, $C_{10}H_{17}N_2O_9^-$, $C_{12}H_6NO_4^-$, and $C_{14}H_{13}O_8^-$ (see the fragmentation pattern in Table S3).

Similar to the styrene SOA, the rule of fragmentation also happened in unique styrene–furan SOA. The parent ions with –COOH group ($C_9H_{11}O_4^-$ (a), $C_{10}H_{15}O_4^-$ (b), $C_{11}H_{11}O_6^-$ (c) and $C_{12}H_{17}O_4^-$ (d)) underwent a neutral loss of CO_2 or H_2O (Table S4), the parent ions with –OH group ($C_9H_{11}O_4^-$ (a), $C_{10}H_{15}O_4^-$ (b), and $C_{11}H_{11}O_6^-$ (c)) underwent a neutral loss of H_2O (Table S4), and the parent ions with –CHO group ($C_{10}H_{15}O_4^-$ (b)) underwent a neutral loss of CO (Table S4). In addition, oligomer $C_{11}H_5O_5^-$ can be decomposed into $C_6H_3O_3^-$ or $C_7H_3O_4^-$ through the ester bond cleavage; likewise, the cleavage of the ester bond also happened in $C_{10}H_{15}O_4^-$ (Table S4).

A simplified chemical mechanism describing SOA production from the OH oxidation of styrene and styrene–furan is proposed in Fig. 6 (red represents the oxidation reaction of styrene, and blue represents the oxidation

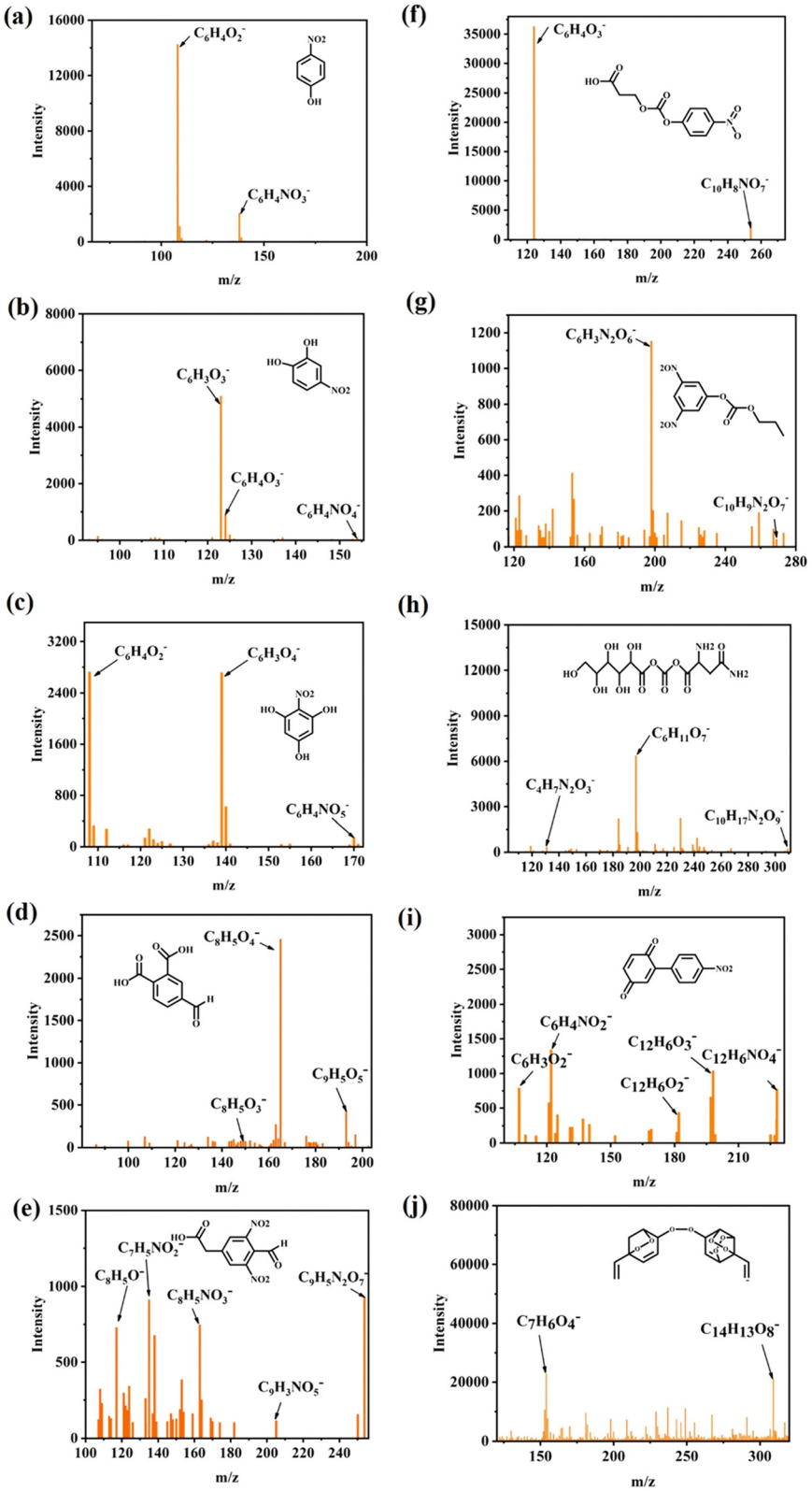

Fig. 5 MS/MS spectra of major compounds for unique styrene SOA in the smog chamber. Monomers: (a) $C_6H_5NO_3$, (b) $C_6H_5NO_4$, (c) $C_6H_5NO_5$, (d) $C_9H_6NO_5$, (e) $C_9H_6N_2O_7$, (f) $C_{10}H_9NO_7$, (g) $C_{10}H_{10}N_2O_7$, and (h) $C_{10}H_{18}N_2O_9$. Dimers: (i) $C_{12}H_7NO_4$ and (j) $C_{14}H_{14}O_8$.

reaction of furan). In the styrene oxidation system, first, OH can abstract H and generate seven intermediates R· (a, b, c, d, e, f, g) (Fig. S13). Second, taking R· (e for styrene) for example, it can react with O_2 to form a series of RO· or RO_2·

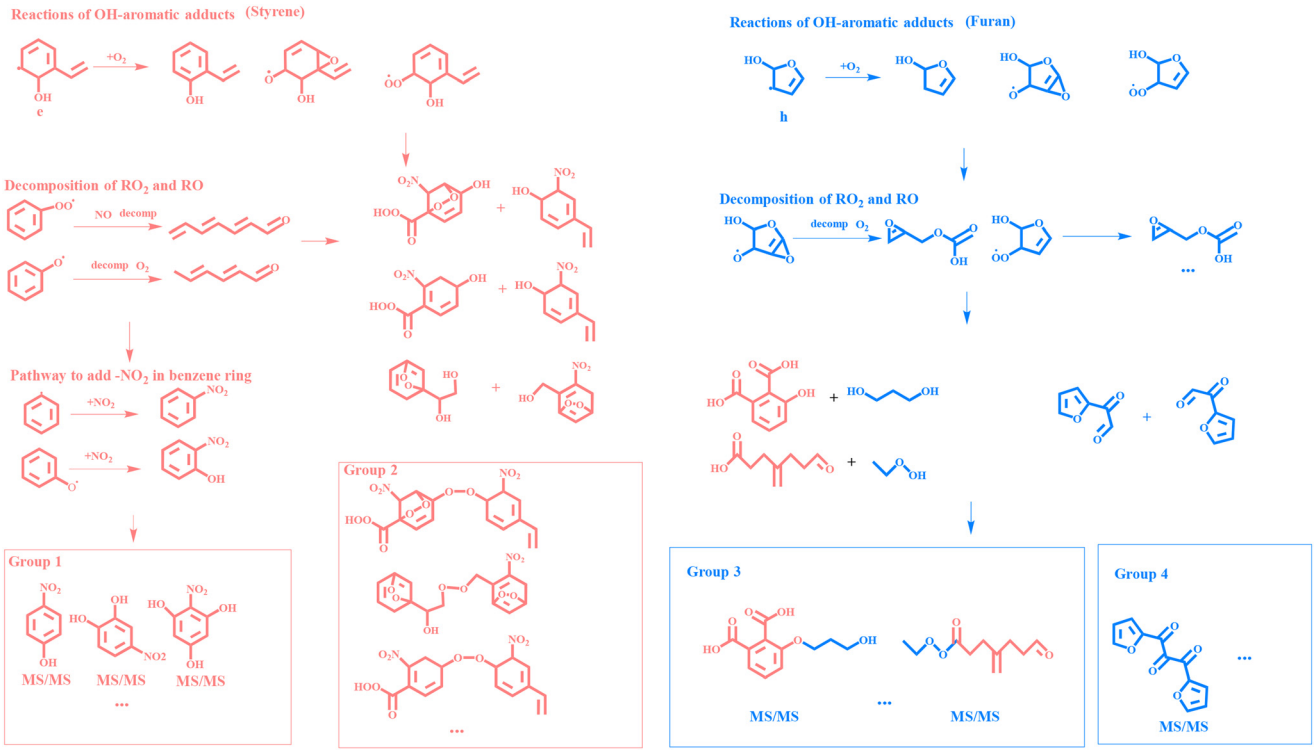

Fig. 6 Simplified formation schemes for the styrene SOA and styrene–furan SOA (the compounds identified by MS/MS have been marked).

(see the reactions of OH–aromatic adducts in Fig. 6). Then, the RO_2· can react with NO and then decompose into carbonyls, and RO· undergo decomposition and addition of O_2, leading to the formation of carbonyl compounds (cyclic RO_2· or RO· can open ring, and long chain RO_2· or RO· can be decomposed into small molecules with short chains). Correspondingly, these RO_2· or RO· radicals generate a series of ROOH or ROH compounds. Subsequently, a range of group 2 products, such as R, ROR, and ROOR, were generated from the reaction of ROOH, RO, or ROH (representative compounds are shown in Fig. 6). It should be noted that these compounds exhibit low volatility, mainly classified as LVOCs or ELVOCs (Table S2). The high light absorption for styrene SOA is mainly attributed to nitrogen-containing compounds, which are from the addition of $–NO_2$ group to the benzene ring[23] (Fig. 6). Correspondingly, the formation processes of representative products (*i.e.*, group 1: identified to be the primary BrC chromophores in styrene SOA) are depicted in Fig. 6.

When furan was introduced into the system, the formation of group 1 products (such as the $C_6H_5NO_3$, $C_6H_5NO_4$, $C_6H_5NO_5$) and group 2 products (dimers in Fig. 6) was suppressed, as indicated by the blue pathway in Fig. 6. In addition to the similar hydrogen abstraction and addition reactions observed for furan, two main mechanisms contribute to this inhibitory effect. First, the reactive intermediates derived from furan can interact with those from styrene to form dimer-like compounds (represented by group 3 products identified by MS/MS), which possess higher volatility than group 1 products. As a result, the overall SOA yield in the furan–styrene system was lower than that in the styrene-only system which consistent with the observed shifts in O/C ratio before. Furthermore, the cross-reactions between furan- and styrene-derived intermediates compete with the reaction between styrene intermediates and NO_2, thereby reducing the formation of nitrogen-containing products that typically exhibit strong light absorption. Second, furan-derived intermediates can also self-react to form relatively more volatile products (group 4 products), further reducing SOA yields in the mixed system.

4. Conclusion

BB emissions are a significant source of various trace gases and nanoparticles. Compared to a single VOC oxidation in previous studies, this study provides new insights into the interactive effects of VOCs in BB emissions, focusing on the co-oxidation of furan and styrene under low and high degrees of oxidation. It was found that the SOA yield and light absorption decreased with the addition of furan compared to styrene SOA under both low and high degrees of oxidation. By comparing the predicted and measured SOA yields as well as *k*-values, we suggest that the addition of furan exerts a molecular-level influence on the formation and optical properties of mixed SOA. Combined with MS/MS spectrometry, we further investigated the molecular-level mechanisms underlying the observed decreases in

SOA yield and light absorption with the addition of furan. The results revealed that the reduction in SOA yield is mainly attributed to the decrease of LVOCs and ELVOCs in mixed system oxidation, which were identified to be nitrogen-containing compounds and dimers. Meanwhile, light absorption reduction was primarily due to the inhibition of nitrophenol formation by furan, since the main nitrophenols (*e.g.*, $C_6H_5NO_3$, $C_6H_5NO_4$, and $C_6H_5NO_5$) were only detected in styrene SOA.

The [styrene]/[furan] ratios studied represent the real-world variability of biomass burning emissions, which depends on fuel type (*e.g.*, lignin-rich woody biomass *vs.* cellulose-rich agricultural residues) and combustion conditions. Consequently, the influence of VOC interactions on SOA properties is spatially and temporally heterogeneous. Specifically, emissions with a high furan/styrene ratio (*e.g.*, from agricultural residue burning[19,22]) will produce SOA whose yield and absorptivity are significantly suppressed by chemical interactions. In contrast, SOA from fuels with a lower ratio (*e.g.*, woody biomass[19,22]) will have properties closer to those predicted from styrene alone. This variability must be considered to accurately assess the impacts of biomass burning.

This study highlights the importance of considering molecular-level interactions between co-emitted VOCs in atmospheric models. Such interactions can significantly alter the predicted SOA yield and optical properties, thereby impacting the role of SOA in atmospheric radiative forcing and air quality in regions influenced by BB emissions. Furthermore, the mechanistic understanding gained from the furan–styrene system offers a generalizable framework. The suppression of SOA yield and light absorption likely extends to other VOC mixtures involving precursors with contrasting chemical characteristics, particularly between aromatic chromophore-forming species (*e.g.*, styrene, phenols) and those yielding more volatile oxidation products (*e.g.*, furans). Prioritizing the study of such functionally distinct VOC pairs will be crucial for systematically improving the representation of SOA formation from complex emissions in atmospheric models.

Author contributions

Shan Zhang: investigation, methodology, data curation, writing – original draft preparation. Kun Li: investigation, supervision, funding acquisition, writing – review & editing. Li Xu: review & editing. Lin Du: instrument supply, review & editing.

Conflicts of interest

The authors declare that they have no known competing financial interests or personal relationships that could have appeared to influence the work reported in this paper.

Data availability

The data of this study are available on Zenodo: https://zenodo.org/records/16894027.

Supplementary information (SI) is available. See DOI: https://doi.org/10.1039/d5en00770d.

Acknowledgements

This work was supported by the National Natural Science Foundation of China (42305100) and the Shandong Provincial Natural Science Foundation (ZR2023QD092).

References

1 S. K. Akagi, R. J. Yokelson, C. Wiedinmyer, M. J. Alvarado, J. S. Reid, T. Karl, J. D. Crounse and P. O. Wennberg, Emission factors for open and domestic biomass burning for use in atmospheric models, *Atmos. Chem. Phys.*, 2011, **11**, 4039.

2 A. Ito and J. E. Penner, Historical emissions of carbonaceous aerosols from biomass and fossil fuel burning for the period 1870–2000, *Global Biogeochem. Cycles*, 2005, **19**, GB2028.

3 M. J. Alvarado, C. R. Lonsdale, R. J. Yokelson, S. K. Akagi, H. Coe, J. S. Craven, E. V. Fischer, G. R. McMeeking, J. H. Seinfeld and T. Soni, *et al.*, Investigating the links between ozone and organic aerosol chemistry in a biomass burning plume from a prescribed fire in California chaparral, *Atmos. Chem. Phys.*, 2015, **15**, 6667.

4 M. J. Alvarado, C. Wang and R. G. Prinn, Formation of ozone and growth of aerosols in young smoke plumes from biomass burning: 2. Three-dimensional Eulerian studies, *J. Geophys. Res.: Atmos.*, 2009, **114**, 0148.

5 A. P. S. Hettiyadura, V. Garcia, C. Li, C. P. West, J. Tomlin, Q. He, Y. Rudich and A. Laskin, Chemical composition and molecular-specific optical properties of atmospheric brown carbon associated with biomass burning, *Environ. Sci. Technol.*, 2021, **55**, 2511.

6 D. E. Romonosky, S. L. Gomez, J. Lam, C. M. Carrico, A. C. Aiken, P. Chylek and M. K. Dubey, Optical Properties of Laboratory and Ambient Biomass Burning Aerosols: Elucidating Black, Brown, and Organic Carbon Components and Mixing Regimes, *J. Geophys. Res.: Atmos.*, 2019, **124**, 5088.

7 A. Hodzic, P. S. Kasibhatla, D. S. Jo, C. D. Cappa, J. L. Jimenez, S. Madronich and R. J. Park, Rethinking the global secondary organic aerosol (SOA) budget: stronger production, faster removal, shorter lifetime, *Atmos. Chem. Phys.*, 2016, **16**, 7917.

8 M. R. Marvin, P. I. Palmer, F. Yao, M. T. Latif and M. F. Khan, Uncertainties from biomass burning aerosols in air quality models obscure public health impacts in Southeast Asia, *Atmos. Chem. Phys.*, 2024, **24**, 3699.

9 L. N. Posner, G. Theodoritsi, A. Robinson, G. Yarwood, B. Koo, R. Morris, M. Mavko, T. Moore and S. N. Pandis, Simulation of fresh and chemically-aged biomass burning organic aerosol, *Atmos. Environ.*, 2019, **196**, 27.

10 J. B. Gilman, B. M. Lerner, W. C. Kuster, P. D. Goldan, C. Warneke, P. R. Veres, J. M. Roberts, J. A. de Gouw, I. R. Burling and R. J. Yokelson, Biomass burning emissions and potential air quality impacts of volatile organic compounds and other trace gases from fuels common in the US, *Atmos. Chem. Phys.*, 2015, **15**, 13915.
11 J. Jiang, W. P. L. Carter, D. R. Cocker, III and K. C. Barsanti, Development and Evaluation of a Detailed Mechanism for Gas-Phase Atmospheric Reactions of Furans, *ACS Earth Space Chem.*, 2020, **4**, 1254.
12 L. D. Yee, K. E. Kautzman, C. L. Loza, K. A. Schilling, M. M. Coggon, P. S. Chhabra, M. N. Chan, A. W. H. Chan, S. P. Hersey and J. D. Crounse, *et al.*, Secondary organic aerosol formation from biomass burning intermediates: phenol and methoxyphenols, *Atmos. Chem. Phys.*, 2013, **13**, 8019.
13 M. Huang, J. Xu, S. Cai, X. Liu, W. Zhao, C. Hu, X. Gu, L. Fang and W. Zhang, Characterization of brown carbon constituents of benzene secondary organic aerosol aged with ammonia, *J. Atmos. Chem.*, 2018, **75**, 205.
14 J. Li, H. Li, K. Li, Y. Chen, H. Zhang, X. Zhang, Z. Wu, Y. Liu, X. Wang and W. Wang, *et al.*, Enhanced secondary organic aerosol formation from the photo-oxidation of mixed anthropogenic volatile organic compounds, *Atmos. Chem. Phys.*, 2021, **21**, 7773.
15 E. U. Emanuelsson, M. Hallquist, K. Kristensen, M. Glasius, B. Bohn, H. Fuchs, B. Kammer, A. Kiendler-Scharr, S. Nehr and F. Rubach, *et al.*, Formation of anthropogenic secondary organic aerosol (SOA) and its influence on biogenic SOA properties, *Atmos. Chem. Phys.*, 2013, **13**, 2837.
16 D. Thomsen, L. D. Thomsen, E. M. Iversen, T. N. Björgvinsdóttir, S. F. Vinther, J. T. Skønager, T. Hoffmann, J. Elm, M. Bilde and M. Glasius, Ozonolysis of α-Pinene and Δ^3-Carene Mixtures: Formation of Dimers with Two Precursors, *Environ. Sci. Technol.*, 2022, **56**, 16643–16651.
17 G. McFiggans, T. F. Mentel, J. Wildt, I. Pullinen, S. Kang, E. Kleist, S. Schmitt, M. Springer, R. Tillmann and C. Wu, *et al.*, Secondary organic aerosol reduced by mixture of atmospheric vapours, *Nature*, 2019, **565**, 587.
18 C. E. Stockwell, P. R. Veres, J. Williams and R. J. Yokelson, Characterization of biomass burning emissions from cooking fires, peat, crop residue, and other fuels with high-resolution proton-transfer-reaction time-of-flight mass spectrometry, *Atmos. Chem. Phys.*, 2015, **15**, 845.
19 M. O. Andreae, Emission of trace gases and aerosols from biomass burning – an updated assessment, *Atmos. Chem. Phys.*, 2019, **19**, 8523.
20 T. Joo, J. E. Machesky, L. Zeng, T. Hass-Mitchell, R. J. Weber, D. R. Gentner and N. L. Ng, Secondary brown carbon formation from photooxidation of furans from biomass burning, *Geophys. Res. Lett.*, 2024, **51**, e2023GL104900.
21 E. A. Bruns, I. El Haddad, J. G. Slowik, D. Kilic, F. Klein, U. Baltensperger and A. S. H. Prévôt, Identification of significant precursor gases of secondary organic aerosols from residential wood combustion, *Sci. Rep.*, 2016, **6**, 27881.
22 E. A. Bruns, J. G. Slowik, I. El Haddad, D. Kilic, F. Klein, J. Dommen, B. Temime-Roussel, N. Marchand, U. Baltensperger and A. S. H. Prévôt, Characterization of gas-phase organics using proton transfer reaction time-of-flight mass spectrometry: fresh and aged residential wood combustion emissions, *Atmos. Chem. Phys.*, 2017, **17**, 705.
23 S. Zhang, K. Li, X. Chen, Z. Yang and L. Du, Molecular composition of secondary brown carbon from styrene at low-to-high oxidation degrees, *Environ. Pollut.*, 2025, **368**, 125795.
24 A. E. R. El Mais, B. D'Anna, L. Drinovec, A. T. Lambe, Z. Peng, J. E. Petit, O. Favez, S. Aït-Aïssa and A. Albinet, Insights into secondary organic aerosol formation from the day- and nighttime oxidation of polycyclic aromatic hydrocarbons and furans in an oxidation flow reactor, *Atmos. Chem. Phys.*, 2023, **23**, 15077.
25 H. Jiang, A. L. Frie, A. Lavi, J. Y. Chen, H. Zhang, R. Bahreini and Y.-H. Lin, Brown Carbon Formation from Nighttime Chemistry of Unsaturated Heterocyclic Volatile Organic Compounds, *Environ. Sci. Technol. Lett.*, 2019, **6**, 184.
26 M. Tajuelo, D. Rodriguez, M. Teresa Baeza-Romero, Y. Diaz-de-Mera, A. Aranda and A. Rodriguez, Secondary organic aerosol formation from styrene photolysis and photooxidation with hydroxyl radicals, *Chemosphere*, 2019, **231**, 276.
27 Z. Yang, N. T. Tsona, C. George and L. Du, Nitrogen-containing compounds enhance light absorption of aromatic-derived brown carbon, *Environ. Sci. Technol.*, 2022, **56**, 4005.
28 X. Ma, K. Li, S. Zhang, Z. Yang, L. Xu, N. Tsona Tchinda and L. Du, Oxidation Flow Reactor and Its Application in Secondary Organic Aerosol Formation in Laboratory Studies, *ACS ES&T Air*, 2025, **2**, 1394.
29 K. D. Lu, F. Rohrer, F. Holland, H. Fuchs, B. Bohn, T. Brauers, C. C. Chang, R. Häseler, M. Hu and K. Kita, *et al.*, Observation and modelling of OH and HO_2 concentrations in the Pearl River Delta 2006: a missing OH source in a VOC rich atmosphere, *Atmos. Chem. Phys.*, 2012, **12**, 1541.
30 F. Rohrer, K. Lu, A. Hofzumahaus, B. Bohn, T. Brauers, C.-C. Chang, H. Fuchs, R. Häseler, F. Holland and M. Hu, *et al.*, Maximum efficiency in the hydroxyl-radical-based self-cleansing of the troposphere, *Nat. Geosci.*, 2014, **7**, 559.
31 A. R. Koss, K. Sekimoto, J. B. Gilman, V. Selimovic, M. M. Coggon, K. J. Zarzana, B. Yuan, B. M. Lerner, S. S. Brown and J. L. Jimenez, *et al.*, Non-methane organic gas emissions from biomass burning: identification, quantification, and emission factors from PTR-ToF during the FIREX 2016 laboratory experiment, *Atmos. Chem. Phys.*, 2018, **18**, 3299.
32 X. Chen, L. Du, Z. Yang, S. Zhang, N. T. Tchinda, J. Li and K. Li, Interaction between marine and terrestrial biogenic volatile organic compounds: Non-linear effect on secondary organic aerosol formation, *Atmos. Environ.*, 2024, **338**, 120868.
33 Q. Liu, J. Liggio, K. Li, P. Lee and S.-M. Li, Understanding the Impact of Relative Humidity and Coexisting Soluble Iron on the OH-Initiated Heterogeneous Oxidation of Organophosphate Flame Retardants, *Environ. Sci. Technol.*, 2019, **53**, 6794.

34 S. Zhang, L. Du, Z. Yang, N. T. Tchinda, J. Li and K. Li, Contrasting impacts of humidity on the ozonolysis of monoterpenes: insights into the multi-generation chemical mechanism, *Atmos. Chem. Phys.*, 2023, **23**, 10809.
35 B. Chu, Y. Liu, Q. Ma, J. Ma, H. He, G. Wang, S. Cheng and X. Wang, Distinct potential aerosol masses under different scenarios of transport at a suburban site of Beijing, *J. Environ. Sci.*, 2016, **39**, 52.
36 F. Bianchi, T. Kurtén, M. Riva, C. Mohr, M. P. Rissanen, P. Roldin, T. Berndt, J. D. Crounse, P. O. Wennberg and T. F. Mentel, *et al.*, Highly oxygenated organic molecules (HOM) from gas-phase autoxidation involving peroxy radicals: a key contributor to atmospheric aerosol, *Chem. Rev.*, 2019, **119**, 3472.
37 Y. Li, U. Poeschl and M. Shiraiwa, Molecular corridors and parameterizations of volatility in the chemical evolution of organic aerosols, *Atmos. Chem. Phys.*, 2016, **16**, 3327.
38 P. Lin, P. K. Aiona, Y. Li, M. Shiraiwa, J. Laskin, S. A. Nizkorodov and A. Laskin, Molecular characterization of brown carbon in biomass burning aerosol particles, *Environ. Sci. Technol.*, 2016, **50**, 11815.
39 D. Cai, C. Li, J. Lin, W. Sun, M. Zhang, T. Wang, M. Abudumutailifu, Y. Lyu, X. Huang and X. Li, *et al.*, Comparative study of atmospheric brown carbon at Shanghai and the East China Sea: Molecular characterization and optical properties, *Sci. Total Environ.*, 2024, **941**, 173782.
40 P. Lin, J. Liu, J. E. Shilling, S. M. Kathmann, J. Laskin and A. Laskin, Molecular characterization of brown carbon (BrC) chromophores in secondary organic aerosol generated from photo-oxidation of toluene, *Phys. Chem. Chem. Phys.*, 2015, **17**, 23312.
41 L. T. Fleming, P. Lin, J. M. Roberts, V. Selimovic, R. Yokelson, J. Laskin, A. Laskin and S. A. Nizkorodov, Molecular composition and photochemical lifetimes of brown carbon chromophores in biomass burning organic aerosol, *Atmos. Chem. Phys.*, 2020, **20**, 1105.
42 PubChem Compound Summary for CID 980, 4-Nitrophenol, National Center for Biotechnology Information, 2024.
43 K. Levsen, H.-M. Schiebel, J. K. Terlouw, K. J. Jobst, M. Elend, A. Preiß, H. Thiele and A. Ingendoh, Even-electron ions: a systematic study of the neutral species lost in the dissociation of quasi-molecular ions, *J. Mass Spectrom.*, 2007, **42**, 1024.
44 X. Fu, Y. Zhang, S. Shi, F. Gao, D. Wen, W. Li, Y. Liao and H. Liu, Fragmentation study of hexanitrostilbene by ion trap multiple mass spectrometry and analysis by liquid chromatography/mass spectrometry, *Rapid Commun. Mass Spectrom.*, 2006, **20**, 2906.
45 A. C. Schmidt, R. Herzschuh, F. M. Matysik and W. Engewald, Investigation of the ionisation and fragmentation behaviour of different nitroaromatic compounds occurring as polar metabolites of explosives using electrospray ionisation tandem mass spectrometry, *Rapid Commun. Mass Spectrom.*, 2006, **20**, 2293.
46 K. Levsen, H.-M. Schiebel, B. Behnke, R. Dötzer, W. Dreher, M. Elend and H. Thiele, Structure elucidation of phase II metabolites by tandem mass spectrometry: an overview, *J. Chromatogr. A*, 2005, **1067**, 55.
47 B. Witkowski and T. Gierczak, Characterization of the limonene oxidation products with liquid chromatography coupled to the tandem mass spectrometry, *Atmos. Environ.*, 2017, **154**, 297.